Journal of the Serbian Society for Computational Mechanics / Vol. 2 / No. 2, 2008 / pp. 16-28

UDC: 519.876.5:669.718

Computational Reconstruction of Scanned Aluminum Foams for Virtual Testing

M. Borovinšek[1*], M. Vesenjak[1], M. Jože[2], Z. Ren[1]

[1] University of Maribor, Faculty of Mechanical Engineering, Smetanova ulica 17, 2000 Maribor, Slovenia
matej.borovinsek@uni-mb.si,
m.vesenjak@uni-mb.si,
ren@uni-mb.si
[2] University Medical Centre Maribor, Ljubljanska ulica 5, 2000 Maribor, Slovenia
**Corresponding author*

Abstract

A procedure for analysis of geometrical features of real metallic open-cell foams using computer tomography and additional image processing is presented. Obtained three-dimensional computer foam model was used for geometrical and structural analysis of the aluminum foam sample. Measurements of foam geometrical features show that its structure significantly differs from the theoretical equilibrium models used in research of liquid foams (soap froth), since solid foams have richer and more diverse distribution of basic cell building blocks. Those findings are also supported by performed computational simulations which were used to analyze the effect of measured cell elongation on the mechanical properties of the foam. Considerable effect on mechanical properties was observed, which suggests that more realistic foam models have to be used to improve the understanding of foam structure effects on their macroscopic properties.

Keywords: aluminum foam, foam geometry, computer tomography, volume thinning, LS-DYNA

1. Introduction

Mechanical properties of metallic open-cell materials (metallic foams – Fig. 1) depend primarily on the properties of used base material and the morphology of the cells. The influence of the base material on the properties of metal foams is well studied and there are many empirically determined relations that link the properties of the base material to the properties of cellular material (Ashby, et al. 2000, Degischer, et al. 2002, Gibson, et al. 1997). Metals and alloys used for metal foams need to have low density to retain the advantage of low relative density over conventional solid materials. Because of this, the most commonly used metals for cellular materials are aluminum, magnesium and titanium and their alloys.

The impact of cell morphology on the mechanical properties of irregular open-cell materials was examined by many authors using the representative unit cell. In doing so the assumption was made that the behavior of the cellular material can be describe well enough with one, geometrically correct cell. Since the cell geometry of the real open-cell foams differs from the geometric regularity, many authors also studied the cell morphology of real foams. The basis for the research of real open-cell foam morphology represents the research of soap froth, which was started by Plateau (1873). However, the solid foams significantly differ from the liquid foams, since their base materials have completely different physical properties. Because of the difference in base material composition and the manufacturing temperature of polymer and metal cellular materials, such materials are produced from much more viscous liquid base as water (soap froth). Thus, the foaming of the liquid base also includes the phenomena of heat transfer, phase change and visco-elasticity. Due to the nature of the basic material, cooling and the phase change effects, the formation of foam nuclei in these foams and their growth significantly differfrom liquid foams. Even more important is the fact that solid foams do not reach the equilibrium state of the foam because of used production methods. Mainly due to the fact that solidification occurs already during the foaming process before the foam reaches the equilibrium state of the liquid foam due to high viscosity and low melting point of the base material. This fact partially neglects the application of liquid foam laws (Plateau laws) for use in research of solid foams. Therefore more in-depth analysis of the solid foam property dependency on the foam morphology is necessary.

First the review of the previous research is given describing the methods used for determining the geometry of real foam samples. Next the methods used in this paper are presented. First, the method for extracting and analyzing the foam geometrical features of the foam from the images obtained by computer tomography is described. Secondly, the method for building the finite element model of the foam sample is presented. The results of the statistical analysis of foam geometry features are analyzed including the size distributions of cell edges, cell windows and cell volumes. Then the engineering stress-strain curves of foam compression from different coordinate directions are generated by using the computational simulations. The relevant conclusions are given at the end.

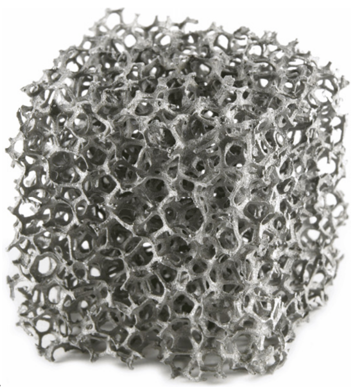

Fig. 1. Aluminum open-cell foam sample.

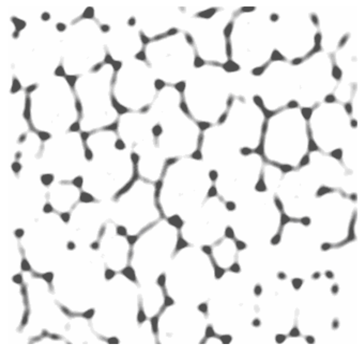

Fig. 2. Cross-section of the sample.

2. Previous research

Measurements of foam geometry were usually made with help of optical inspection, photography or optical microscopy. Especially the techniques of optical microscopy are suitable for measurements of foam geometry. Geometric properties such as thickness of cell walls, cell diameter and length of the cell edges can be measured (Rhodes, et al. 1985, Richardson, et al. 1986). Good results are also obtainable using confocal microscopy (Hamza, et al. 1996).

However, due to the complex 3D structure of foams such manual measurements of their features are tedious, require a lot of time and in the vast majority of cases also include the destruction of the sample. In addition, some foam features (cell volume) are extremely difficult to measure or to determine using such techniques. Consequently, there is very little experimental research and data that describes the correlation between the morphological foam features and macroscopic physical properties of real foams. It is known that the size of the cells and their geometric irregularity affects the macroscopic foam properties (Badiche, et al. 2000, Mukai, et al. 1999), but the proper modeling of real foams is still impossible due to the lack of data of their real morphology.

Better results, than manual measurement methods, provide automated computer image analyses of two-dimensional (2D) images. Using such methods the time required for measurement of foam geometric features is reduced to a negligible value in comparison with the time required for manual analysis. However, the first studies with computer image analysis included only measurements of one of foam geometric properties at a time. Because of different methods and procedures that were used to measure even the most basic geometric foam features, such as the diameter of the cell, the direct comparisons of such results is not possible. The results of those studies can not be combined in a single foam model to obtain a comprehensive insight into the foam structure, so it is necessary to use a method for more complete characterization of foam structure.

Complete characterization of geometric foam features enables an accurate and proportionate 3D computer model of real foam. A number of measurements, such as the length of cell edges, the number of cell window edges or the cell diameter can be carried out on such proportional model instead of measuring the real foam sample. But the measurements on the proportional model instead of using the real foam sample can only be done if the model is large enough (includes a sufficient number of measured geometric features) and reliable. Such models can be obtained through 3D image scanning techniques such as magnetic resonance (Gonatas, et al. 1995) or computer tomography using X-rays (Montminy, et al. 2004) with the subsequent analysis of the resulting 3D images.

However, the problems in the 3D image analysis, such as the presence of noise in the scanned images, limitations of computer memory and processing power prevented the first attempts to cover large enough foam samples to become a recognized tool for analyzing foam samples. Kose (1996) used nuclear magnetic resonance to scan the sample of polyurethane foam and through analysis of resulting 3D images detected 8 polyhedral cells. Monnereau, et al. (1998) reconstructed 9 liquid foam cells (bubbles) of soap froth analyzing images obtained by optical tomography. Cenens, et al. (1994) did not directly search for individual cells, but they evaluated the cell density through analysis of cell edge statistics and form the shape and position of cell windows. In this study the assumption was made that the cell windows are located precisely in the middle between two centers of adjacent cells. This is not the case in real foams, especially in foams with large difference in cell sizes (polydisperse foams).Montminy, et al. (2004) used computer tomography with X-rays to create 3D images of polydispese polyurethane foam samples and built a proportional computer foam model using 3D image processing technique called volume thinning. With this method they reconstructed a total of 376 cells foam six real foam samples. That sufficed for performing the statistical analysis of foam geometric features on the proportional computer foam model. A similar procedure was applied in the presented study to reconstruct the structure of real metal foam.

The reconstructed foam structure vas used for analysis of foam geometrical features such as cell edge lengths, size of internal angles, cell window areas and cell volumes since those features greatly impact the behavior of the foam under external load. Measurements showed anisotropic cell elongation in the foam sample which is a result of the foam production process.

In order to show the effect of cell elongation on the mechanical properties of the foam sample the digitalized foam model was subjected to compressive loads from three different directions by means of explicit dynamic simulations.

3. Materials and methods

The paper presents a statistical and mechanical analysis of an open-cell aluminum foam Duocel. The average cell size of the sample is 5 mm (5 ppi), the relative density of the sample is ρ_r = 7 % (Fig. 1). The sample was analyzed using computer tomography with X-rays, where the 3D image was obtained by means of mathematical reconstruction from the set of 2D images (slices). The computer tomograph Toshiba-Aquilion 64 was used for this task. The resolution in the cross-section plane was 0.12 mm and the distance between individual slices was 0.3 mm. One of the aluminum foam sample slices is shown in Fig. 2, where dark and bright pixels represent a basic foam material and foam voids, respectively.

3.1 Image analysis methods

3D images obtained by computer tomography or magnetic resonance contain a large amount of information on the geometrical features of foam, but procedures for extracting this information are complex. For this purpose a software package was designed to visualize and analyze the geometric structure of the open-cell foams from 3D images.

The first step of foam geometry analysis represents a decision, which voxels of the 3D image represent the basic foam material and which represent foam voids. This step is called segmentation in the analysis of 3D images. Obtained 3D image is namely composed of slices with 8-bit color depth (256 colors), which have to be reduced to binary images for the reconstruction of the scanned volume. 3D Binary image or the volume model is an image where voxels with value 1 (black) represent the solid volume of cellular material and voxels with value 0 (white) represent foam voids. Acquiring an accurate 3D binary image is very important, since the 3D image segmentation determines where in the image space the base material of the foam is located and where are the voids. The boundary surface between black and white voxels is very important for the identification and analysis of the foam geometry. It also represents the basis for the creation of the foam surface model (Fig. 3). The surface model was generated using the algorithm called "marching cubes" for the purpose of 3D image verification and the possibility of comparison with other developed models described later.

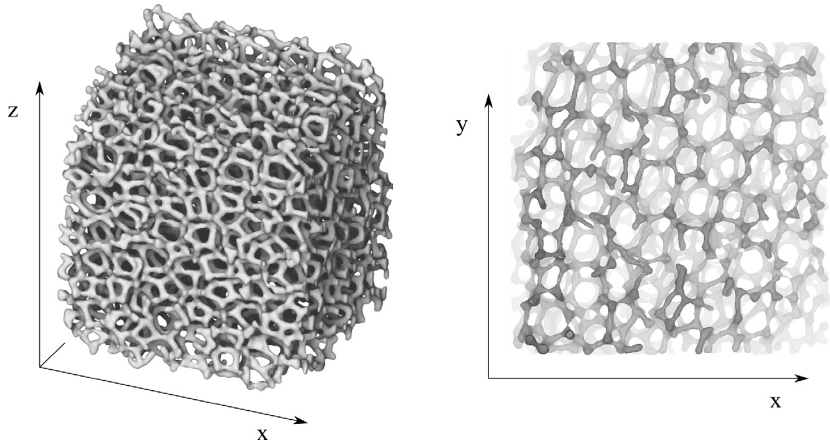

Fig. 3. Foam surface model (left isometric view; right view from the top).

In the next step of the foam analysis a topological model is generated from the volume model. Topological model is used to obtain the majority of the geometrical features present in the volume model, which includes positions of cell edges, windows and cells of the cellular structure of the foam. Topological model is generated from a volume model using the image processing method called volume thinning. This method gradually removes outer layers of voxels of the volume model until the structure reaches a thickness of one voxel. Used algorithm (Xie, et al. 2003) ensures that the resulting topological model maintains connectivity from the volume model and that the resulting skeleton is located as close as possible to the center line of a volume model (Fig. 4).

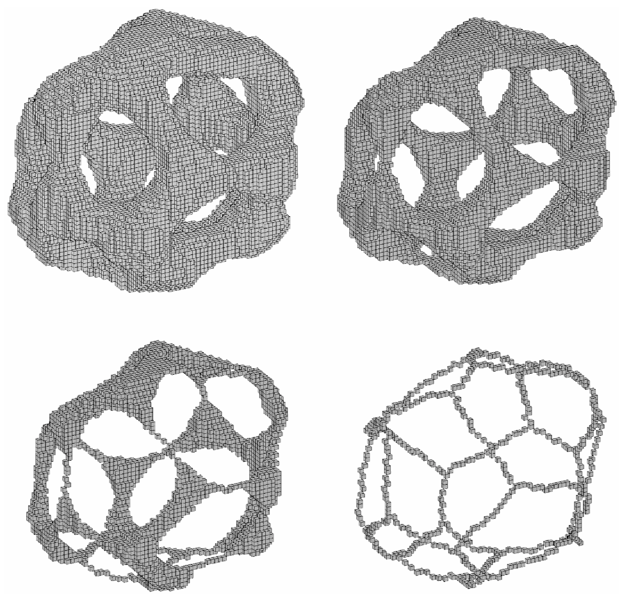

Fig. 4. The process of volume thinning of one foam cell.

A lattice model is then created from the topological model (Fig. 5). First the edge vertices (joints) in the topological model are identified. They are represented by voxels which are connected with at least three other neighboring voxels. The connectivity of identified joints is determined next by using the method of breadth-first search. The edge between two selected joints exists, if those joints are connected through voxels in such a way, that no other joints are between them. This results in the lattice model of the foam, which contains the positions of the joints and appropriate connections between them (edges). The resulting lattice model contains some geometric distortions caused by the noise in the scanned images and by the foam geometry imperfections. Thickened edge joints can result in two or more separate joints in the topological model at the position where the volume model has only one joint. However, the distance between these joints is very small and such imperfections can be removed using automatic model smoothing. Obtained edge connectivity is used for next breadth-first search to find edges that form a cell window and later to find windows that form cell. The results of described image analysis method are foam models, which are directly based on the positions of cell edges in obtained 3D image. This ensures the accuracy and reliability of such models in respect to the structure of real foam. Fig. 6 shows the comparison between the lattice and volume model of the selected foam sample. Produced lattice models include all geometric features of the foam and are thus used for measuring the foam geometry and creation of the finite element model.

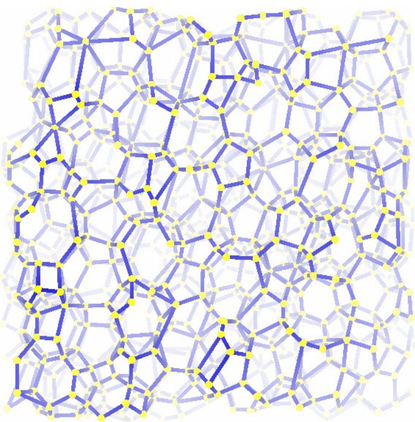

Fig. 5. Lattice model of the foam.

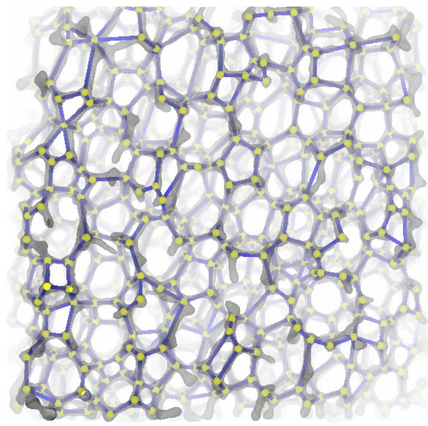

Fig. 6. Overlay of the surface and lattice models of the foam.

3.2 Finite element model

Computational simulations of open-cell foam behavior under impact loading (uni-axial compression) were performed using dynamic explicit finite element code LS-DYNA. All computational simulations were performed using the same foam model subjected to impact loading from three different coordinate directions.

Finite element model of the foam was based on the lattice foam mode. Cell edges in the lattice model were meshed using linear beam elements, since LS-DYNA incorporates only beam elements of linear form. To capture the micro-buckling of cell edges, which is the dominant mechanism responsible for the failure of the open-cell foams in compression (Gan, et al. 2005), longer cell edges were discretised by several beam elements. Two criteria were used for discretisation. The first criterion was the maximum number of linear beam elements on a single cell edge, which was set to 3 and the second criterion was that the shortest element in the finite element mesh after the division should have the same length as before the division (time step). The result is the finite element mesh where cell edges are modelled using one, two or three linear beam elements, depending on the edge length. The circular beam cross-section shape was used with a radius r, which was determined from the relative foam density ρ_r, total length of all beam elements L_{tot} and a specimen volume V by using the equation:

$$r = \sqrt{\frac{\rho_r \cdot V}{\pi \cdot L_{tot}}} \tag{1}$$

For the base material of the analyzed open-cell foams the aluminium material properties were used, where the ideal elasto-plastic characteristic was assumed. Young's modulus was set to E = 70 GPa, Poison's ratio to ν = 0.35 the density to ρ = 2.7 t/m^3 and the yield stress to σ_y = 250 MPa.

Two additional plates were modelled at the bottom and the top side of the open-cell mesh. First plate was used to apply the compressive load through a prescribed motion and the second plate to offer support for the compressed foam. Steel material properties with elastic characteristic were used for the plate material with the shell thickness set to 1 mm. All degrees of freedom were fixed by the nodes of the support plate, while the load plate nodes were free to move only in the direction normal to the plate.

Contact conditions were defined between the plates and the open-cell foam model. To assure the convergence and stability of the performed impact simulations, some amount of friction had to be applied. The required minimum value of friction coefficient was determined by preliminary simulations. In order to keep the open-cell mesh during compression in place a friction coefficient of k = 0.01 suffices. The contact between deformed cell edges was simulated using a second contact definition between beam finite elements with a friction coefficient of k_{Al} = 0.50. The Coulomb approximation of fiction was used in both contact definitions.

4. Results of image analysis

A geometry analysis of described aluminum foam sample Duocel was carried out. The results of the analysis of scanned 3D image of the Duocel foam sample are 5,735 identified cell edges, which meet at 14,258 internal angles, form 2963 cell windows and 179 closed cells (Table 1). All measured geometry features were statistically analyzed by computing their average value f and standard deviation σ. Based on this parameters the features distribution plots were generated showing the number of samples (frequency) in respect to the value of analyzed feature. The width of the intervals was set to one standard deviation.

4.1 Sample description

Duocel foam sample had a cube shape with the outer dimensions of 39.5 x 39.5 x 40.5 mm. The volume of the entire sample was 63,190 mm^3, while the measured volume of the foam base material equaled 4500 mm^3. Calculated relative density of the sample was 7.12 %. The sample was scanned using a resolution of 0.12 x 0.12 x 0.30 mm, the resulting slice images were used to build a 3D image with a resolution of 333 x 333 x 333 voxels using linear interpolation between slices.

4.2 Cell edge lengths

There were 5,735 cell edges identified and measured in the sample. Calculated average cell edge length is 3.32 mm, the distribution of cell edge lengths is shown in Fig. 7. Clearly, the cell edge lengths deviate more towards cell edges greater than the average, giving the right asymmetric distribution, which is typical for natural systems and in good correlation with previous results (Montminy, et al. 2001). Optical inspection of the foam sample shows, that cells of the foam are not evenly sized in all coordinate directions. Comparing the lengths of cell edge projections on the coordinate axes (Fig. 3) gives the following length ratio $lx : ly : lz = 0.852 : 1 : 0.828$. The length ratio obviously shows the effect of gravitational and production forces on the structure of foam sample, since analyzed foam sample was obviously elongated in the y coordinate direction. The effects of foam elongation on the mechanical properties of the foam are be presented later.

4.3 Internal angles

External load on the open-cell materials is directly transferred to cell edges and their joints. For this reason the internal angle analysis can deliver important findings of the foam behavior under load. The distribution of 14,258 identified internal angles between cell edges is shown in Fig. 8. The average angle between internal edges is 104.63º and is smaller but close to the expected equilibrium angle of 109.5°. This is the angle between four cell edges in the equilibrium foam structure, as described by Plateau (1873). Other authors have also measured the average internal angle that is smaller than the equilibrium one. There are several reasons for the deviation from the Plateau laws. The first reason is that the solid foam is not the equilibrium structure as mentioned in the introduction. Such foams namely solidify before they can relax to the equilibrium state. The second reason is the manufacturing process, during which the solidifying foam is subjected to external forces. For this reason the surface tension is not the only driving force defining the foam structure. Additionally, joints with more than four cell edges can be found in the real foam. The internal angles between cell edges in such joints are smaller than in the theoretical foam. Only few such edge joints in the foam reduce the average internal angle.

4.4 Window area and shape

Many properties of the open-cell materials depend on the size of the windows between the cells (fluid flow). In this analysis 2963 windows were identified, with the distribution of their surface shown in Fig. 9. The area of the window was calculated as the sum of the triangle areas, which form the window, since windows rarely (except triangular windows) lay in one plane. Distribution of window areas is also right asymmetric, similar to the distribution of edge lengths. The reason is that the window area size and consequently its distribution originate from the cell edges sizes. There were 122 identified triangles, 755 quadrilaterals, 1664 pentagons, 404 hexagons, 16 heptagons and 2 octagons. Table 2 shows the comparison between the results of the performed analysis and data from the literature (Montminy, et al. 2004). Clearly, the analyzed foam has much more diverse cell window shapes in comparison with theoretical models based on the assumption of the minimum surface area (Kelvin, Weir-Phelan). Comparing the results to liquid foam analyses (Matzka, Kose) a similarity between can be observed, however these results already deviate from the idealized foam models. The last two results are from the analyses of the solid foams and both strongly deviate from other results. While presented study analyzed features of aluminum foam, Montminy, et al. (2004) studied polymer foams. Despite larger difference in cell sizes the cell size distributions are very similar, reflecting the common characteristics of solid foams and particularly their deviation from the ideal theoretical shape.

4.5 Cell volume and shape

The volume of cells was calculated as the sum of pyramid volumes witch have the cell window at their base and the cell center at their top. In the foam sample 179 closed cells were identified and measured. The average cell volume was 100.79 mm^3 and the average number of windows per cell was 13 (Table 1). Assuming the spherical shape of the cells the average cell diameter would equal to 5.77 mm. The distribution of cell volumes (Fig. 10) and the size ratio between the smallest and the largest cell (15.13 : 152.03) indicate that this is a foam with a large variety of cell sizes whose properties would be difficult if not impossible to describe using simplified models with representative unit cell.

5. Results of computational simulations

The effect of the cell shape elongation on the compressive behavior of the open-cell foam sample was studied by means of computational simulations. For this reason the scanned open-cell foam was discretised with finite elements and computationally subjected to compressive dynamic loading from three different coordinate directions x, y and z. During the deformation the reaction forces and deformations were measured from which Young's modulus, tangent modulus and engineering stresses-strain curves were calculated.

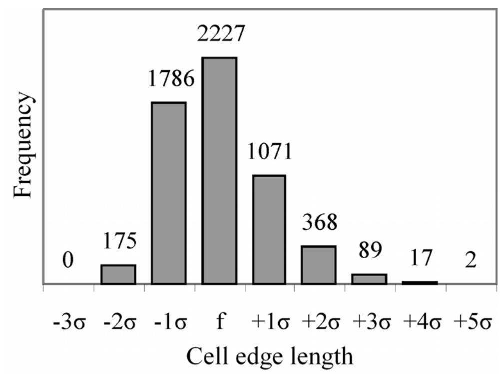

Fig. 7. Distribution of cell edge lengths.

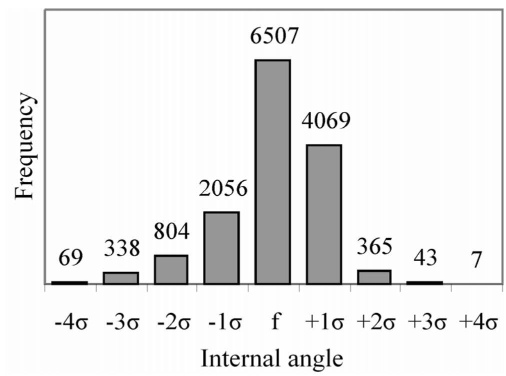

Fig. 8. Distribution of internal angles.

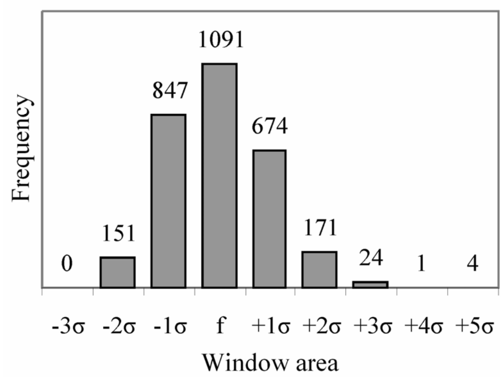

Fig. 9. Distribution of windows areas.

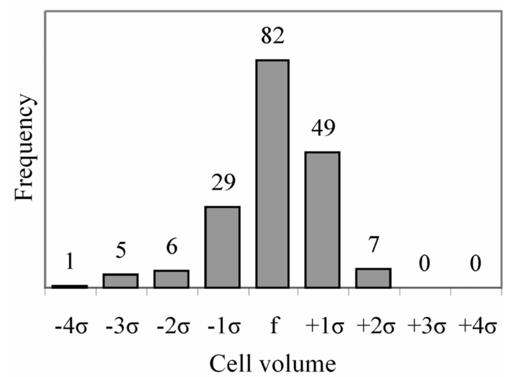

Fig. 10. Distribution of cell volumes.

Since the deformation behavior of all simulated load cases is visually very similar only the deformation sequence of compression in x is shown in Fig. 11. To make the deformation behavior more evident the figure represents a slice of the whole model. The slice thickness is about one quarter of the model. The compression starts with an elastic deformation of the model. Then a plastic deformation of cells in contact with loading and supporting plate (at the top and bottom of the model) occurs. Those cells were cut when the sample was prepared to get a cubic shape and because of that their load carrying capacity was lowered. After that a plastic deformation begins by plastic hinge formation and cell collapse in narrow, localized bands similar to the deformation behavior observed in two-dimensional Voronoi foam models (Silva, et al. 1997). Once a deformation band is formed, deformation further proceeds by localization band propagation spreading over the entire model. These bands are oriented at an angle of about 30° in respect to supporting plates and spread through entire model reflecting the underlying quasi-periodic structure of the model. This angle is also close to the orientation of shear bands in an isotropic incompressible elastoplastic material under plane stress conditions, where the shear bands are oriented at an angle of 35.26° (Badiche, et al. 2000).

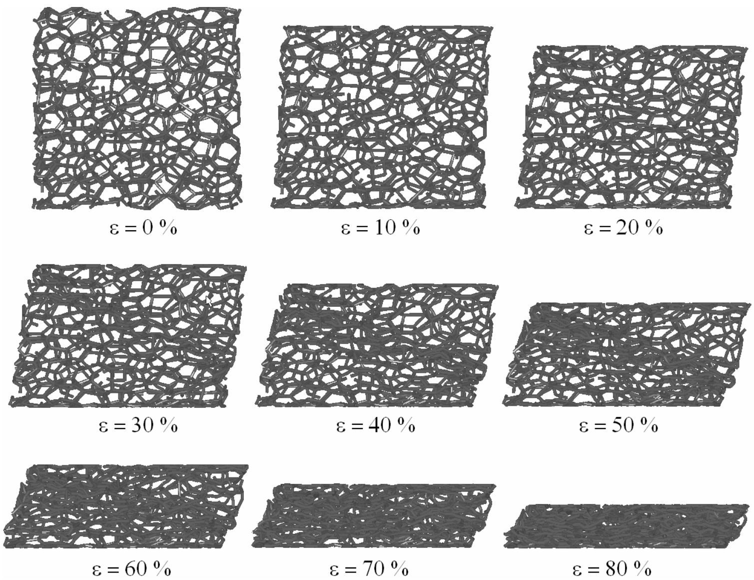

Fig. 11. Simulated compression behavior of scanned foam sample in x direction.

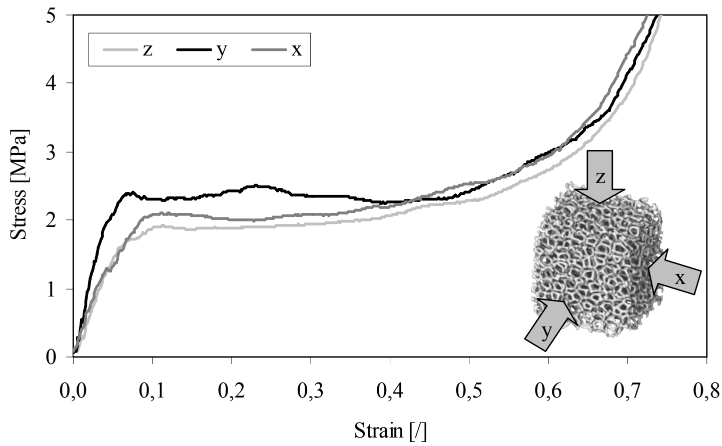

Fig. 12. Engineering stress-strain curves for compression in x, y and z direction.

Computationally generated engineering stress strain curves for all three load cases are shown in Fig. 12, Young's and tangent modulus and normalized strain energy are presented in Table 1. Stress-strain curves were calculated from measured force-displacement data with the assumption of constant cross-section perpendicular to the load direction. Stress-strain diagram shows expected shape of stress-strain curves with large Plateau stress region, where energy is absorbed at almost constant stresses and the densification of the foam at higher strains. The effect of cell elongation on mechanical properties is also clearly evident. The elastic stresses and Plateau stresses of y-compression are evidently higher than stresses by x or z-compression up to the start of densification. After the start of densification the differences become smaller and curves eventually merge. These observations are confirmed by values of parameters of mechanical properties given in Table 1, where tangent modulus describes the foam behavior between strains of 10 and 50 %, and strain energy represent the area under the stress-strain curve up to a specific strain. The y-compression results in higher Young's modulus and higher strain energy. The tangent modules are more difficult to compare, since the plastic deformation path largely depends on model irregularity.

The reason for simulated results is the elongation of cells in the scanned sample. Detected elongation of the cells affects the mechanical properties in two different ways. Firstly, elongated cells have different compressive load carrying capacity depending on the load direction. Compressive load carrying capacity is greater in the direction of the elongation and smaller in the direction perpendicular to it. The elongation of the cells can be seen as a pre-deformation of the structure in the opposite way of work load thus, increasing the strength of the structure. Since the cells in the sample were elongated in the direction of y-axis, this results in higher mechanical properties. And secondly, elongated cells have smaller cross-sections perpendicular to the elongation. Because of that more cells are needed to fill the sample in cross-section perpendicular to y-axis. More cells again result in larger load carrying capacity of the simulated foam in y-direction.

Compression direction	Normalized cell elongation	Young's modulus [MPa]	Tangent modulus [MPa]	Normalized strain energy at $\varepsilon = 60\%$ [/]
x	**0.852**	**33.143**	**1.011**	**0.909**
y	**1.000**	**58.061**	**-0.182**	**1.000**
z	**0.828**	**33.952**	**1.046**	**0.843**

Table 1. Computed mechanical properties of aluminum foam sample for different compression directions.

6. Conclusions

Image analysis results show that an automatic 3D analysis of the geometrical features of real metallic open-cell foams can be done by combination of several methodologies. The geometric features distributions of the analyzed sample give an important insight into the foam structure. It turns out that the geometric features of solid foams are not similar to the theoretical but have a rich and diverse distribution of basic cell building blocks. Since solid foams are not equilibrium structures, they are very different from the regular structures based on tetrakaidekahedral or cubic cell, which are used as basis in many research studies.

Computer simulations were used to confirm image analysis results. It was shown that in order to capture the compression behavior of open-cell foam their real geometrical features have to be taken into account. The results show far greater load carrying capacity of the simulated foam sample in the cell elongation direction. The Young's modulus was increased up to 75 % and impact energy absorption capacity was up to 8 % higher. Taking into account that this are the results for the same foam sample with the same mass, the increase in mechanical properties is quite prominent. Further research and modeling of open-cell metal foams thus needs to be based on irregular real structures to improve the understanding of foam structure effects on their macroscopic properties.

Development of improved real open-cell models allows further research of foam geometrical structures and their impact on the macroscopic physical properties of foams. Of great interest are especially foam modeling and compressive load analysis and also fluid flow analysis through the foam. There is also a benefit for the foam producers, since new findings may improve the foam production quality und usability and enable the development of new products.

References

Ashby MF, Evans A, Fleck NA, Gibson LJ, Hutchinson JW and Wadley HNG (2000). Metal foams: a design guide. Elsevier Science, Burlington, Massachusetts.

Degischer HP and Kriszt B (2002). Handbook of cellular metals. Wiley-VCH Verlag GmbH & Co. KGaA,

Gibson LJ and Ashby MF (1997). Cellular solids: structure and properties. Cambridge University Press, Cambridge.

Plateau J (1873). Statique Experimentale et Theorique des Liquides Soumis aux Seules Forces Moleculaires. Gauthier-Villars, Paris.

Rhodes MB and Nathhorst RP (1985). Stereological analysis of foams with a computer interfaced optical microscope. Proc. American Institute of Chemical Engineers, National Meeting, Houston, TX, USA

Richardson MOW and Nandra DS (1986). Cell size determination of polymeric foams, Cellular Polymers, 5, 6, 423-431.

Hamza R, Zhang X-d, Macosko CW, Stevens R and Listemann M (1996). Imaging open cell foam via confocal microscopy. Proc. American Chemical Society, Polymer Priprints, Division of Polymer Chemistry, Orlando, FL, USA

Badiche X, Forest S, Guibert T, Bienvenu Y, Bartout JD, Ienny P, Croset M and Bernet H (2000). Mechanical properties and non-homogeneous deformation of open-cell nickel foams: application of the mechanics of cellular solids and of porous materials, Materials Science and Engineering A, 289, 1-2, 276-288.

Mukai T, Kanahashi H, Miyoshi T, Mabuchi M, Nieh TG and Higashi K (1999). Experimental study of energy absorption in a close-celled aluminum foam under dynamic loading, Scripta Materialia, 40, 8, 921-927.

Gonatas CP, Leigh JS, Yodh AG, Glazier JA and Prause B (1995). Magnetic resonance images of coarsening inside a foam, Physical Review Letters, 75, 3, 573.

Montminy MD, Tannenbaum AR and Macosko CW (2004). The 3D structure of real polymer foams, Journal of Colloid and Interface Science, 280, 1, 202-211.

Kose K (1996). 3D NMR Imaging of Foam Structures, Journal of Magnetic Resonance - Series A, 118, 2, 195.

Monnereau C and Vignes-Adler M (1998). Optical tomography of real three-dimensional foams, Journal of Colloid and Interface Science, 202, 1, 45-53.

Cenens J, Huis R, Chauvaux B, Dereppe JM, Gratin C and Meyer F (1994). 3D cellular structure characterization of flexible polyurethane foam. Proc. American Society of Mechanical Engineers, Materials Division (Publication) MD, Chicago, IL, USA

Xie W, Thompson RP and Perucchio R (2003). A topology-preserving parallel 3D thinning algorithm for extracting the curve skeleton, Pattern Recognition, 36, 7, 1529-1544.

Gan YX, Chen C and Shen YP (2005). Three-dimensional modeling of the mechanical property of linearly elastic open cell foams, International Journal of Solids and Structures, 42, 26, 6628-6642.

Montminy MD, Tannenbaum AR and Macosko CW (2001). New algorithms for 3-D imaging and analysis of open-celled foams, Journal of Cellular Plastics, 37, 6, 501-515.

Silva MJ and Gibson LJ (1997). The effects of non-periodic microstructure and defects on the compressive strength of two-dimensional cellular solids, International Journal of Mechanical Sciences, 39, 5, 549-563.